The need to monitor the release of ultrafine particles and airborne carbon nanotubes during mechanical recycling of lithium-ion batteries

Supporting Information

Part, Florian [1], Sparwasser, Kevin [2,] *, Falta, Thomas [3], Jandric, Aleksander [1], Szakács, Zoltán [2], Wong, Marilyn [1], Pavlicek, Anna [4], Bieri, Ruedi [2], Van Kerckhove, Gunther [5]

[1] BOKU University, Department of Landscape, Infrastructure and Water, Institute of Waste Management and Circularity, Muthgasse 107, 1190 Vienna, Austria

[2] Stat Peel Ltd., Stampfgasse 4, CH-8750 Glarus, Switzerland

[3] Austrian Workers‘ Compensation board (AUVA), Head Office, Prevention, Vienna Twin Towers, Wienerbergstraße 11, 1100 Vienna, Austria

[4] BOKU University, Department of Biotechnology and Food Science, Institute of Synthetic Bioarchitectures, Muthgasse 11/II, 1190 Vienna, Austria

[5] OCSiAl Europe Sarl, Rue de la Poudrerie 1, 3364 Leudelange, Luxembourg

* Corresponding author: Kevin.Sparwasser@statpeel.com

S1 – Material composition of LFP cells, type 'Edge575'

Table S1. Material composition of the LFP cells used in this study.

LFP cell with SWCNTs (average total weight = 1938 g)					
Cathode [wt%]			Anode [wt%]		
1.60	PVDF	Polyvinylidene fluoride	1.20	CMC	Carboxymethyl cellulose
0.45	CB	Carbon black	96.45	Graphite	
0.27	*TUBALL™ BATT NMP*	SWCNTs	2.25	SBR	Synthetic polybutadiene rubber
97.38	LFP	$LiFePO_4$	0.10	*TUBALL™ BATT H_2O*	SWCNTs
0.30	Dispersant	Not specified			
LFP cell with MWCNTs (average total weight = 2034 g)					
Cathode [wt%]			Anode [wt%]		
1.60	PVDF	Polyvinylidene fluoride	1.50	CMC	Carboxymethyl cellulose
0.45	CB	Carbon black	95.50	Graphite	
0.55	*Cnano*	MWCNTs	2.00	SBR	Synthetic polybutadiene rubber
97.10	LFP	$LiFePO_4$	1.00	CB	Carbon black
0.30	Dispersant	Not specified			

S2 – Sample preparation

The prismatic cells with an aluminium casing had a length of 575 mm, a width of 108 mm, and a thickness of 17 mm. For this study, 40 test cells with MWCNTs and 30 test cells with SWCNTs were provided and each cell was weighed. The MWCNT cells showed an average weight of 2034 g (1.03% RSD), the SWCNTs cells had 1938 g (1.40% RSD). The applied steps in sample preparation prior to the simulated recycling processes are listed below and the results are summarized in Figure S1:

1. Weighting and documentation: Each cell was weighed and photographed prior to further dismantling.
2. Opening the metal casing: The metal casing of the cell was cut open with using pliers and a metal saw along the shorter side of the cell.
3. Removal of active material: The active material, including the plastic foil cover, was then removed from the metal casing.
4. Cutting the plastic foil cover: The plastic foil cover was cut open to remove cathode and anode sheets, and the separator foil.
5. Resulting battery cell components: Each cell component, including individual cathode and anode sheets, was weighed and counted.
6. Storage: The resulting components were stored separately until further testing.

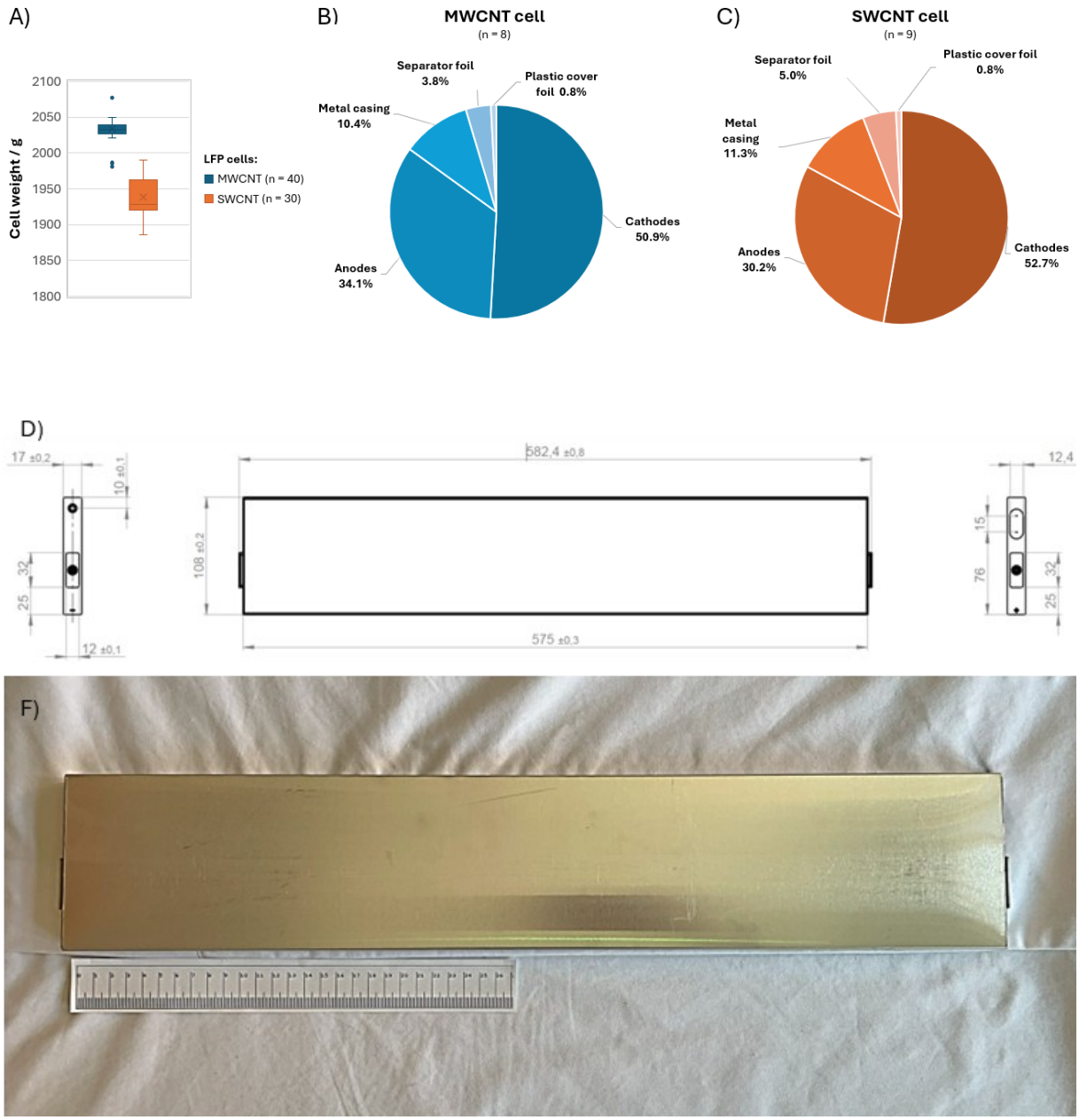

Figure S1. Average cell weight (A) and main components in weight percentage (wt%) of a MWCNT cell (A) and a SWCNT cell (B) tested in this study. (D–F) Dimensions in mm of an LFP cell with an aluminium casing.

S3 – Developed protocol to simulate mechanical processing

A mechanical treatment test was designed to mirror real-world recycling practices as closely as possible. The objective of the mechanical treatment was to produce powder material with a particle size of less than 0.5 mm, composed of mixed cathode and anode material, typically referred to as black mass, that is further processed during metallurgical recycling.

The input material for the mechanical treatment was cathode and anode sheets separated by cell type, obtained after an in-depth dismantling process. The mechanical treatment comprised two steps: shredding the material to a particle size of less than 1 cm, followed by milling to achieve a particle size of less than 0.5 mm. The equipment used for the mechanical treatment is shown in Figure S2.

Figure S2. Left image: Shredder (Retsch SM 2000) for reducing the particle size to < 1 cm. Right image: Ultra centrifugal Mill (Retsch ZM 200) for reducing the particle size to < 0.5 mm.

The simulated shredding process began with setting up a sample collection bin, performing an overall shredder inspection, and putting into position a container with cathode and anode sheets without separator foil of one entire battery cell. The material was introduced to the shredder by random handfuls from the container ranging between several segments up to several sheets of anode and cathode material (Figure S3). Due to the volume constraint, the sample collection bin needed to be exchanged twice per shredding process, i.e., in the middle and at the end of the shredding process. After the completion of the shredding process, the resulting shredded cathode and anode material was stored, and the shredder was dusted, cleaned, inspected, and made ready for the next shredding sequence. It took approx. 30 min. to complete the shredding sequence of all anodes and cathode sheets for one cell, including storage of the output fraction, cleaning, and preparation for the next sequence. In total, 5 MWCNT cells and 5 SWCNT cells were shredded as the basis for the milling step to a particle size < 0.5 mm. The detailed shredded time plan is shown in Table S2.

Figure S3. Left image: Shredder feed, which was one folded cathode or anode sheet at the time. Right image: Shredder output fraction after 1 hour of milling, which was used for further comminution.

Table S2. Detailed time plan of shredding MWCNT and SWCNT to particle size <1 cm using a cutting mill. It is important to note that aerosol measurements were conducted for each event.

Shredding < 1 cm			
LFP cell type	**Events**	**Measurement period**	**SMPS runs***
MWCNT cells	1st event	12:43 - 12:49	6
MWCNT cells	2nd event	12:50 - 13:00	10
MWCNT cells	3rd event	13:02 - 13:12	10
SWCNT cells	1st event	15:03 - 15:13	10
SWCNT cells	2nd event	15:15 - 15:25	10
SWCNT cells	3rd event	15:28 - 15:38	10
SWCNT cells	4th event	16:00 - 16:10	10
SWCNT cells	5th event	16:12 - 16:22	10
SWCNT cells	6th event	16:26 - 16:36	10

* The OPS and aerosol CNT sampling devices measured continuously during an event period.

The final size reduction of shredded cathode and anode material to a particle size of < 0.5 mm was carried out using the centrifugal mill. Since this mill has a smaller capacity, the shredded material had to be homogenized, and samples were then taken using a systematic sampling method.

To ensure a representative sample and minimize bias, a systematic sampling plan was developed for the MWCNT and SWCNT cells separately. The process involved two stages: quartering and increment collection, followed by the homogenization step. The detailed process plan is shown in Table S3.

Table S3. Overview of the homogenisation and increment collection of the shredded sample. It is important to note that aerosol measurements were conducted during this sampling event.

Systematic sampling stage	Description
Preparation	The entire shredded cathode and anode material of 5 single-type cells, i.e., MWCNT and SWCNT separately, was collected in a large container and thoroughly mixed manually
1st Partitioning	After the shredded material (~8.79 kg) had been mixed and homogenised, the contents of the container were separated into two piles of roughly equal size (see Figure S4)
1st Increment collection	Ten increments with a mass on average between 30-40 g each were collected from each pile using a hand shovel (see Figure S4)
Mixing and homogenisation	The residual material from the two piles was collected again in a large container, thoroughly mixed and homogenised
2nd Partitioning	The mixed residual material was than separated again into two piles of roughly equal size, following the same principle as in the first partitioning.
2nd Increment collection	Ten increments with a mass on average between 30-40 g each were collected from each pile using a hand shovel, following the same principle as in the first increment collection
Final mixing and homogenisation	The material from 20 increments with a mass of approx. 1 kg was thoroughly mixed and homogenised and placed in a single sample container
Milling sample	The obtained homogenised sample (~ 1kg) was ready for the milling to a particle size <0.5 mm in an ultra-centrifugal mill

Figure S4. Applied homogenisation process of the shredded test cells. Step 1 and 2: Collecting and mixing of all shredded cathode and anode materials from a single cell type. Step 3 and 4: Separating the total shredded material of one cell type. Step 5: Increment collection with a hand shovel.

The milling process was carried out using a ultra-centrifugal mill with a 0.5 mm conical sieve, resulting in an output fraction of < 0.5 mm particle size. The mill was operated at 16,000 revolutions per minute (rpm) without the suction option to simulate conditions like a typical recycling facility. A portion of homogenised shredded cathode and anode sample of a single cell type was taken with the hand shovel from the sample container and gradually introduced to the mill (Figure S5). Due to the volume constraint, the sample collection tray needed to be exchanged approx. every 15 min of milling (Figure S5). The milling of ~ 1 kg of shredded material took 2.5–3 hours. After milling the entire sample of one cell type, the whole sample apparatus of the mill was disassembled, cleaned, and reassembled for the next milling process. The detailed milling process time plan is shown in Table S4.

Figure S5. Left image: Input of shredded material into the centrifugal mill to simulate the production of black mass during the comminution of end-of-life LIBs. Right image: Emptying the sample collection tray.

Table S4. Detailed milling process time plan of shredded MWCNT and SWCNT cells to a particle size < 0.5 mm using an ultra-centrifugal mill. It is important to note that aerosol measurements were conducted for each event.

Milling < 0.5 mm			
LFP cell type	**Name**	**Measurement period**	**SMPS runs***
MWCNT cells	1st event	11:46 - 11:53	7
MWCNT cells	2nd event	13:47 - 13:57	10
MWCNT cells	3rd event	14:10 - 14:20	10
MWCNT cells	4th event	14:38 - 14:48	10
SWCNT cells	1st event	16:07 - 16:17	10
SWCNT cells	2nd event	16:36 - 16:46	10
SWCNT cells	3rd event	17:01 - 17:10	10

* The OPS and aerosol CNT sampling devices measured continuously during an event period.

S4 – Derived nano- and process-specific release rate and factor

Regarding emission or material flow modelling, we derived average battery type- and process-specific release rates and factors of UFPs based on the SMPS measurement results. The UFP release rate (RR_{UFP}) was calculated using the arithmetic mean of the total particle number concentration per SMPS measurement event. The RR_{UFP} is therefore expressed in the total amount of released UFPs per hour (#/h). The UFP release factor (RF_{UFP}) is the sum of particles recorded during the effective commissioning of the mill using SPMS divided by the input quantity of battery materials. Therefore, the RF_{UFP} is expressed as the total amount of UFPs released per 1kg of processed battery input material (#/kg). The RR_{UFP} could be helpful for emission modelling, life cycle assessment or as an initial guidance value for designing air filter systems in recycling facilities. The RF_{UFP} could be a useful partitioning or transfer coefficient for material flow analysis. The results are summarized in the table below.

Table S5. Battery type- and process-specific release rates and factors for ultrafine particles (UFPs) or nanomaterials (RR_{UFP} and RF_{UFP}, respectively) derived from SMPS measurements.

Recycling process	LFP cell type	RR_{UFP} [#/h]	RF_{UFP} [#/kg]
Shredding < 1 cm	MWCNT cells	42547	2735
	SWCNT cells	81352	98430
Milling < 0.5 mm	MWCNT cells	45074	30049
	SWCNT cells	955133	477566

S5 – Selective measurement of airborne CNT concentrations: Method validation and discussion

Current state-of-the-art and limitations

Methods for monitoring occupational exposure to CNTs in the air must have sufficient selectivity to clearly distinguish CNTs from other airborne particles, since working environments usually contain a wide variety of airborne particles. This means that particle counters alone are unsuitable for the quantitative assessment of CNT concentrations. In addition to isotope (C^{13}) labelling combined with mass spectrometry, electron microscopy and thermal analysis techniques, Raman spectroscopy can be used to quantify CNTs in complex environmental matrices (Dresselhaus et al., 2005; Dresselhaus et al., 2010; López-Lorente et al., 2013; Petersen et al., 2016; Saito et al., 2011; Salzmann et al., 2007).

Regarding OHS in industrial settings, the current state-of-the-art and recommended method to assess CNT mass concentrations in the United States is NIOSH Method 5040 (Zumwalde et al., 2013). Originally developed for particulate diesel exhaust monitoring, the method can be used to analyse CNT-containing filter samples. Filter punches are measured in a thermal-optical carbon analyser to obtain the organic and elemental carbon (OC/EC) content of a sample. The determined amount of EC is used as a measure of CNT content, if the determined concentration is found to be significantly elevated compared to the background. Latest instruments are reported to reach a quantification limit of 1 ng/mm^2 carbon on filter, corresponding to a 960-liter air sample taken at about 1 µg/m^3 airborne carbon concentration collected on a 37-mm filter. The quantification limit does not allow monitoring CNT concentrations below the REL at 1 µg/m^3. The method further lacks selectivity for different EC allotropes, hence can inherently not distinguish CNTs from, for example, carbon black or graphite, which commonly co-occur in battery-related workplaces.

In cases where the EC concentration exceeds the REL, NIOSH recommends turning to NIOSH method 7402 adjusted for the measurement of CNT and carbon nanofibers by transmission electron microscopy (Birch et al., 2017). This method involves a sample transfer, i.e., a fraction of the collected dust (e.g. one quarter of the filter) is transferred from the filtration substrate to a TEM grid as quantitatively as possible. Regarding quantitation of fibers, it should be considered that transferring the sample involves assumptions about filter deposit homogeneity and sample transfer efficiency, which may both result in quantification bias and additional uncertainty. For instance, diffusion samples allow the analyte to be collected directly onto a TEM grid, as demonstrated by Tsai and Theisen (2018). However, it should be noted that such samples are not included in the NIOSH Method 7402.

To date, jurisdictions have been reluctant to implement fiber number-based exposure limits for biopersistent nanofibers, largely because there is no consensus about how to consistently assess fiber number concentrations. Difficulties arise from the fibers' small size, complexity, and variety of structures in aerosol samples, including agglomerations of CNTs and matrix materials, as demonstrated in Figure S7 using SEM. Electron microscopy-based methods, such as NIOSH Method 7402, ASTM D8526-23, or VDI Guideline 3492, rely on reproducible visualisation, identification, categorisation and counting of fibrous morphologies. The Federal Institute for Occupational Safety and Health (BAuA) in

Germany has recently developed a statistical SEM-based approach for compliance checking of fiber number concentrations down to a cut-off diameter of 20 nm (Meyer-Plath et al., 2020). The proposed workflow currently involves 1.5-6 h of SEM time and 2-9 h of image analysis per filter sample, while object recognition and categorisation are largely user-dependent. Further work is needed to decrease the workload per sample, standardise and automate fiber recognition to increase consistency, to eventually lower the cost per analysis.

In the following Section, we propose and validate a new method that employs a Stat Peel Identifier C2 system to selectively quantify CNTs from occupational environments. In this study, we present the method's strengths and drawbacks and discuss how it may overcome the shortcomings of state-of-the-art methods for airborne nanofiber quantification.

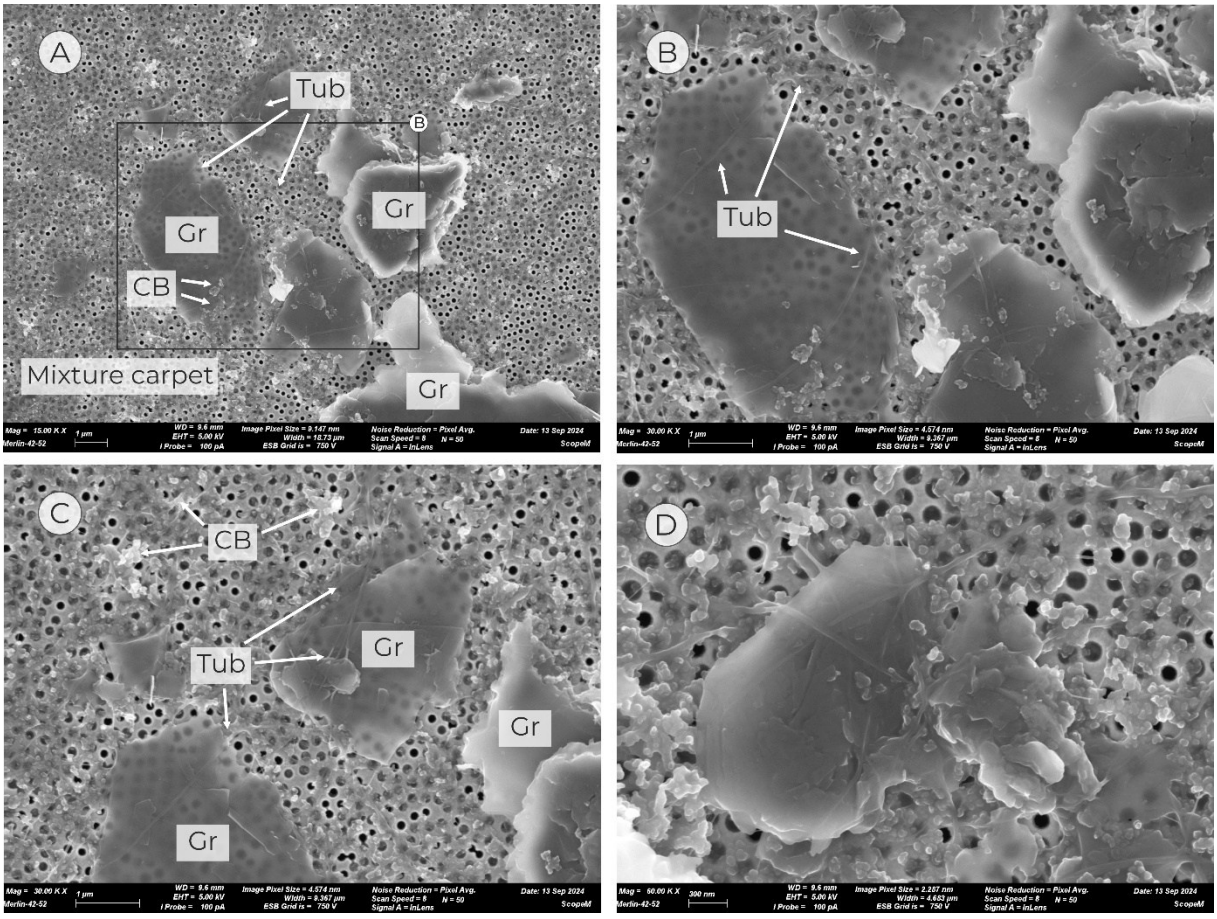

Figure S6. SEM images taken from the sample containing 1 ng Tuball™ SWCNT and 200 ng 1:9 CB/graphite matrix. CB: carbon black; Gr: graphite; Tub: Tuball™ SWCNT.

Stat Peel Identifier C2 system validation

Stat Peel air sampler

The Identifier C2 system uses respirable air samplers ('badges') that were experimentally validated following the validation scheme described in EN 13205-2:2014 (CEN, 2014). For this study, the sampling efficiency was assessed in a calm air chamber using a polydisperse test aerosol (CRM BCR-070, EU Community Bureau of Reference) with a measured mass mean diameter of 3.8 µm and a geometrical standard deviation (GSD) of 1.7. Two optical aerosol spectrometers (sample and reference probe; DustDecoder 11-D, GRIMM Aerosol Technik, Durag Group, Germany) were used to determine particle number concentrations as a function of particle size. The resulting sampling efficiency (Figure S7A) from nine repeated measurements closely matches the respirable convention according to ISO 7708:1995 (ISO, 1995) and has a 50% cut-off size (d_{50}) at 4.4 µm. The corresponding bias iso-map (Figure S7B) reveals a consistently negative sampling bias relative to the respirable convention for commonly encountered aerosol size distributions in occupational environments. The bias is below -10% for 93% of the 216 tested aerosol size distributions. Following the validation scheme described in EN13205-2, the combined sampling standard uncertainty was calculated to be $u_{sampling}$ = 11.7% (cf. Table S8), which represents the uncertainty of measurement originating from the air sampling part of the Stat Peel Method.

Table S6. Major uncertainty components related to air sampling contributing to usampling.

Component	**Source**	**Uncertainty (%)**
Master flow meter calibration	Test certificate	1
Pump rate reading	Test certificate	2
Sampling time	ISO 20581	0.24
Calibration of sampler test system	EN 13205	2
Estimation of sampled concentration	EN 13205	2
Bias rel. to sampling convention	Calculated from exp. data	7.1
Individual sampler variability	EN 13205	7
Excursion from nominal flow rate	EN 13205	5
Combined sampling standard uncertainty $u_{sampling}$		**11.7**

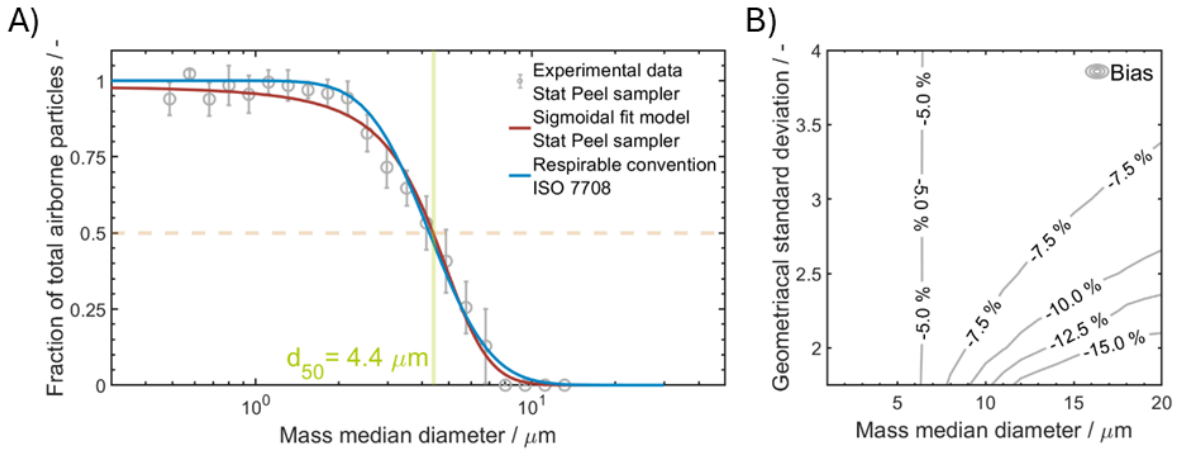

Figure S7. A) Experimentally determined sampling efficiency of Stat Peel Identifier C2 system (sampling 'badge). The data was fit with a sigmoidal fit model (red curve) for comparison to the respirable convention (blue curve) according to ISO 7708:1995. Error bars denote the standard deviation from nine repeated measurements. B) Calculated sampler bias map relative to respirable convention at nominal flow rate of the Badge (0.091 lpm).

CNT quantification with Raman spectroscopy

Stat Peel's Identifier C2 employs Raman spectroscopy for the selective quantification of materials in dust samples. Raman spectroscopy is a non-destructive vibrational spectroscopy technique that provides fingerprint-like information about the material investigated by collecting photons inelastically scattered by the material. The high selectivity makes Raman spectroscopy one of the most used methods for material identification (Smith and Dent, 2019).

The Identifier C2 was validated for measurement of SWCNT and MWCNT using two well-characterized, and widely-used commercial CNTs: Tuball™ SWCNT (OCSiAl, Luxembourg), and NC7000™ MWCNT (Nanocyl, Belgium). The linear instrument working range was determined to be from 0.013 – 25 ng for SWCNT, and 0.27 – 25 ng for MWCNT, respectively. The lower limits of the instrument working range equal the method's limits of quantification (LoQ). Limits of detection (LoDs) and quantification (LoQs) were determined in accordance with ISO 11843-2:2000. For SWCNTs, the LoD and LoQ were 0.004 ng and 0.013 ng, respectively, while for MWCNTs the corresponding values were 0.09 ng and 0.27 ng. The LoQs were calculated from the estimated LoDs following IUPAC recommendations, whereby the LoQ is approximated as three times the LoD (Currie, 1999).

Figure S8 shows the Raman spectra of Tuball™ SWCNT, NC7000™ MWCNT, as well as two further inorganic carbon allotropes, graphite and carbon black, which commonly co-occur with CNTs in sampling environments in battery production or recycling. The four spectra exhibit significant overlap of their G-band (~1590 cm^{-1}), as well as the D-band (~1300 cm^{-1}). However, a closer inspection of the spectra reveals significant differences between the materials in terms of G/D band height ratio, band

width, and, to a minor degree, band centre position. These parameters can be used to selectively identify different carbon allotropes.

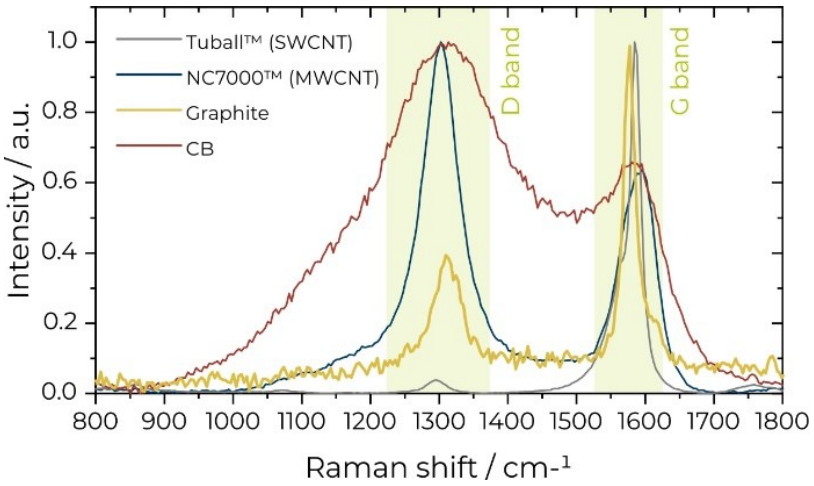

Figure S8. Background-subtracted and normalized Raman spectra of Tuball™ SWCNT, NC7000™ MWCNT, graphite, and carbon black obtained with an Identifier C2 instrument.

Figure S8 shows normalised spectra to illustrate the spectral overlap. The experimentally obtainable Raman intensity depends on a material's Raman scattering cross section, i.e. probability that Raman scattering occurs when the material is illuminated with monochromatic light. There is a lack of literature addressing the differences in Raman scattering cross sections of different carbon allotropes, likely due to the difficulty of their experimental determination. From experience, however, we find that the Raman scattering cross section of SWCNTs is at least 2-3 orders of magnitude higher, and that of MWCNT is at least 1 order of magnitude higher than the matrix carbonaceous materials studied here (CB or graphite). Figure S10 shows the effect of different scattering cross sections by means of relative Raman signal intensities estimated from the measurement of 1 ng SWCNT, MWCNT, carbon black, and graphite. This difference shows that considerably higher amounts of carbonaceous matrix must be present in a sample compared to the CNT target analyte to become significant, i.e. might impair the CNT quantification by introducing a bias.

We investigated the quantitative bias in quantifying SWCNT and MWCNT introduced by the presence of a carbonaceous matrix. Carbon black (CB) and graphite were used as matrix components in a mixing ratio of 1:9. Both materials are expected interferences in air samples collected in battery production/recycling environments, where graphite is anticipated to occur more frequently as it is the main component of anodes in LIBs, and CNTs and CB are used as additives in lower amounts (Hasegawa & Noda, 2016; Liang et al., 2019). For both types of CNT, spiked matrix blank samples were prepared at four masses along the instrument working range. The 1:9 CB/graphite matrix was kept constant at a nominal mass loading of 200 ng, corresponding to matrix-to-CNT ratios between 8 – 4000 (SWCNT), and 8 – 400 (MWCNT). The ratio range is expected to encompass commonly encountered ratios in battery workplace environments. CNT mass loadings in LIBs produced on a lab scale are typically in

the range of 0.2 – 5 wt% (Hasegawa & Noda, 2016; Landi et al., 2009; Li et al., 2006; Wang et al., 2011; Yoo et al., 2019), while commercial manufacturers have incentives to lower the CNT content further to reduce the price. SEM images obtained from spiked matrix samples revealed that all materials were well-dispersed and mixed (Figure S6).

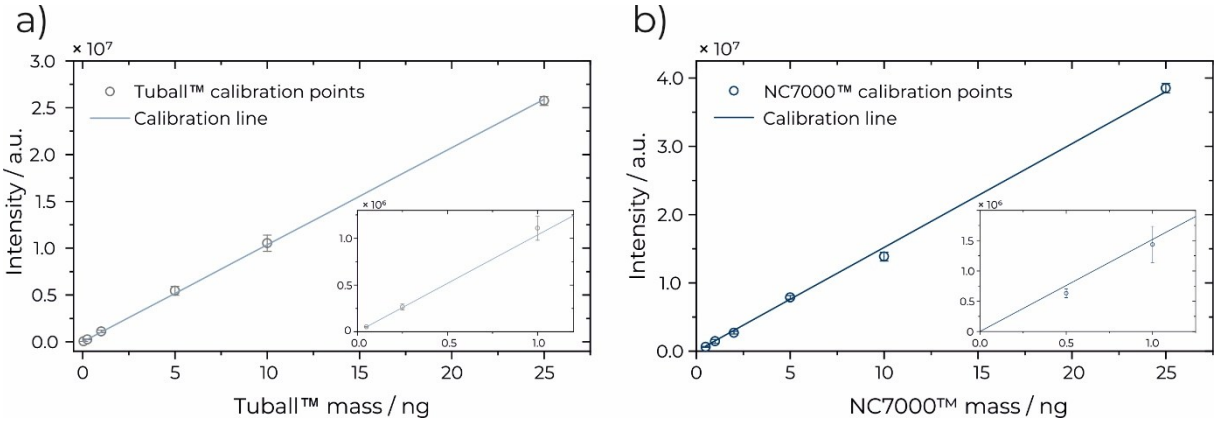

Figure S9. Linear calibration series for Tuball™ SWCNT (a) and (b) NC7000™ MWCNT reference materials. The blue curves are linear regressions in the data range 0.05 – 25 ng (SWCNT) and 0.5 – 25 ng (MWCNT), respectively ($R^2 = 0.999$). The slope of the linear regression is 1.035×10^6 a.u./ng and 1.519×10^6 a.u./ng. The insets are zoom-ins on the lower range of the calibration series. The error bars represent the standard deviation of the averaged signal intensities from three independent standard calibration series.

For the Tuball™ reference material the experimental data showed a linear signal response with mass and the corresponding relative standard deviations (RSD) were in the range of 1.9 - 12.0%. The data were fit with a linear regression model with a fixed intercept at zero. The blue line in Figure S9a shows the linear fit result, a line with a slope of 1.035×10^6 a.u./ng. The coefficient of determination R^2 was determined to be 0.999. The relative errors (RE) in the mass range between 0.05 - 25 ng are below 8% and randomly distributed around zero, confirming the linear signal response to mass in the investigated range.

For the NC7000™ reference material the experimental data showed a linear signal response with mass and the corresponding relative standard deviations (RSD) were in the range of 1.8 - 20.8% with a tendency to become smaller with increasing nominal mass. The data were fit with a linear regression model with a fixed intercept at zero. The blue line in Figure S9b shows the linear fit result, a line with a slope of 1.519×10^6 a.u./ng. The coefficient of determination R2 was determined to be 0.999. The relative errors (RE) in the mass range between 0.5 - 25 ng are below 17% and randomly distributed around zero, confirming the linear signal response to mass in the investigated range.

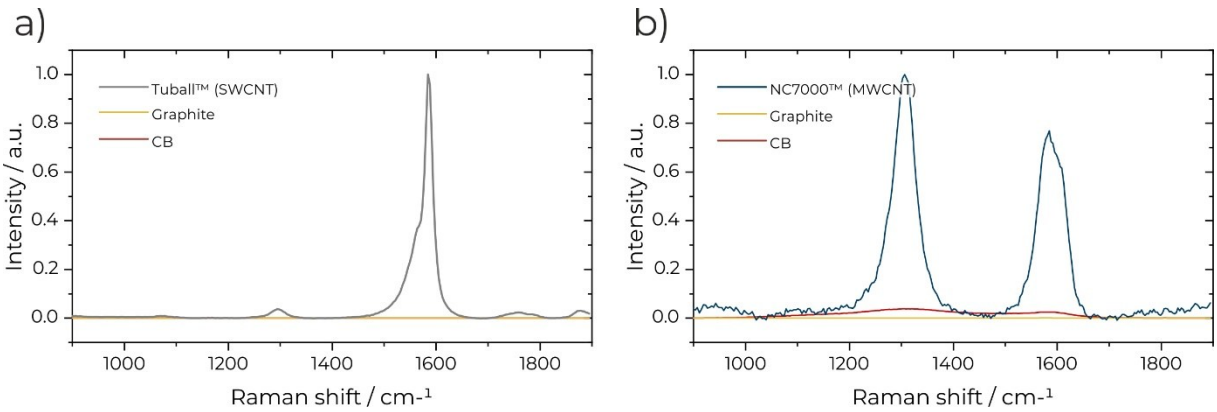

Figure S10. Background subtracted Raman spectra of (a) SWCNT and (b) MWCNT, carbon black, and graphite. The relative intensities were estimated from the measurements of 1 ng material. First, each spectrum was individually normalized to 1, then, divided by the total area of Raman peaks in a given spectrum and multiplied by the slope of their calibration curves. Finally, the obtained relative intensity spectra were normalized to 1 using the same normalization factor with each spectrum shown in a given plot.

Figure S11 shows the quantification results of the spiked matrix samples (see results in Table S8 and Table S9). In the case of SWCNT, the presence of a carbonaceous matrix results in an increased measurement RSD along the entire instrument working range. While the relative error (RE, i.e. bias) remains low in the intermediate mass range (4.0 and 5.2%), a negative bias is observed at the lower and upper end of the instrument working range. The bias at the lower end can be understood in terms of the high matrix-to-CNT ratio. The negative bias at the upper end, however, originates less from insufficient peak decomposition, but rather from membrane overloading and consequent light absorption during the measurement, resulting in a decreased Raman intensity detected. Due to MWCNT's broader band and lower scattering cross section compared to SWCNT, they are expected to be subject to a comparatively higher bias. Figure S11B shows a systematic positive bias in the recovered masses relative to the nominal mass value below 25 ng (26.9 – 75.8%). The bias decreases with increasing mass, reflecting the increasing quality of the spectral decomposition with increasing mass. At high matrix-to-CNT ratios, part of the overlapping Raman band from the CB/graphite matrix can be attributed to MWCNT and results in the observed mass overestimation.

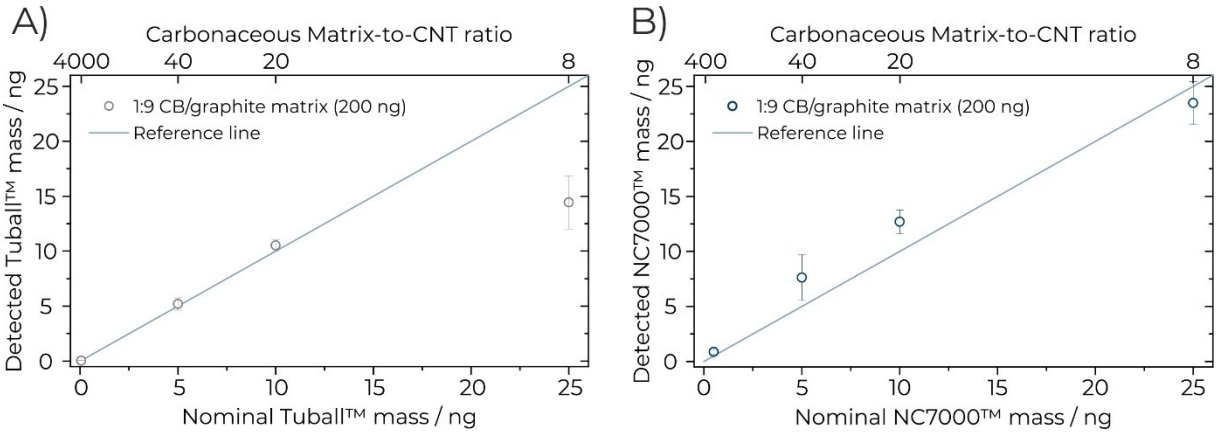

Figure S11. Quantitative bias assessment for Tuball™ SWCNT (A) and NC7000™ MWCNT (B) using spiked matrix blank samples with a 1:9 CB/graphite matrix with a nominal mass loading of 200 ng. Error bars represent the standard deviation of the mean calculated mass from ten repeated measurements. The reference lines denote the ideal CNT recovery factor of 1.

Table S7. Summary of relative standard deviations (RSD) and relative error (RE) with nominal mass for pure SWCNT, and SWCNT in a 200 ng 1:9 CB/graphite matrix.

Nominal mass (ng)	RSD (%)	RE (%)	Matrix-to-CNT ratio	Mean mass (ng)	RSD (%)	RE (%)
	Pure SWCNT		Bias assessment			
0.05	8.3	2.3	4000	0.041	19.9	-18.8
0.25	12.0	3.2	800	-	-	-
1	11.7	7.2	200	-	-	-
5	8.8	5.5	40	5.20	10.7	4.0
10	8.1	1.7	20	10.52	5.3	5.2
25	1.9	-0.5	8	14.43	16.7	-42.3

Table S8. Summary of relative standard deviations (RSD) and relative error (RE) with nominal mass for pure MWCNT, and MWCNT in a 200 ng 1:9 CB/graphite matrix.

Nominal mass (ng)	RSD (%)	RE (%)	Matrix-to-CNT ratio	Mean mass (ng)	RSD (%)	RE (%)
	Pure MWCNT		Bias assessment			
0.5	11.6	-16.9	400	0.9	23.3	75.8
1	20.8	-5.6	200	-	-	-
2	6.9	-11.0	100	-	-	-
5	3.2	3.6	40	7.6	27.3	52.4
10	4.7	-8.8	20	12.7	8.1	26.9

The bias originating from the spectral overlap of multiple carbonaceous species showed an increase towards higher matrix-to-CNT ratios. Particularly, the measurement of MWCNT is affected by a positive bias that results in an overestimated MWCNT concentration, which may guide an industrial hygienist to take a more conservative approach. The highest bias value of 75.8% (matrix-to-MWCNT ratio 400) is a major accuracy improvement compared to NIOSH Method 5040, which would result in a 400-fold CNT overestimation when measuring the same sample.

Note that in this validation study, the fit models of the matrix components did not include any specific lineshape function for their description. Thus, the work demonstrates the real method performance when 'unknown' carbon allotropes are present in the matrix. Improved results could have been achieved in the bias measurements if lineshape functions for graphite and carbon black were included in the fit models (with highly restricted width, center, and peak ratio parameters).

Method working range

The final method working range may coincide with the previously determined instrument working range, however, it must be verified if measurements at all masses along this range are compliant with the uncertainty requirements for measurements for comparison with limit values. ISO 20581:2016 (ISO, 2016) specifies that the method expanded uncertainty must not exceed 50% for long-term samplings in the concentration between 0.1 – 0.5 times the limit value (here NIOSH REL for CNTs at 1 µg/m^3), while it should remain below 30% in the range 0.5 – 2 times the limit value.

The uncertainty of the mass quantification analysis was estimated from the RSD of two components which were considered to contribute directly to the analytical uncertainty, which is calculated by formula (3): (i) RSD of repeated measurements of the identical sample under repeatability conditions. This component represents the uncertainty related to the instrumental capabilities. (ii) The RSD of slopes of the linear regression of the three independent linear standard calibration series used to calibrate the analytical instrument. This component represents the uncertainty related to the nominal mass of the prepared calibration standard samples.

The two components are given as RSD and are standard uncertainties of the corresponding quantity. The two uncertainty contributions are combined according to the method outlined in the EURACHEM/CITAC Guide CG 4.10 (Williams & Ellison, 2012).

(3) $$u_{analytical} = \sqrt{u_{prec}^2 + u_{mass}^2}$$

where $u_{analytical}$ denotes the analytical uncertainty, u_{prec} the uncertainty component estimated as the RSD of precision measurements, and u_{mass} the uncertainty component estimated as the RSD of the standard calibration series fit slope (Figure S12 and Table S9).

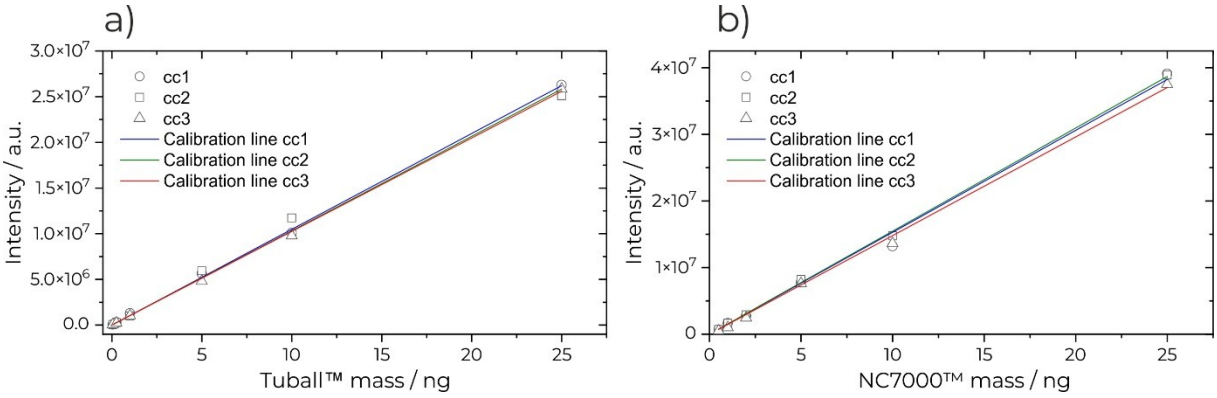

Figure S12. Individual Tuball™ SWCNT (a) and NC7000™ MWCNT (b) calibration curves (cc1-cc3). Coefficient of determination R^2 is better than 0.996 for all linear fits. The corresponding slopes of the fit using a linear regression model are summarized in Table S9.

Table S9. Determined fit slopes of calibration standard series (Figure S12) using a linear regression model with a fixed intercept at zero. RSD of slopes is used a u_{mass}, as further explained in the main text.

Standard calibration series	**Slope of linear fit (a.u./ng)**	**Slope of linear fit (a.u./ng)**
	SWCNT	**MWCNT**
1	1.048×10^6	1.530×10^6
2	1.033×10^6	1.547×10^6
3	1.024×10^6	1.481×10^6
RSD of slopes / u_{mass}	1.0 %	1.8 %

The combined method uncertainty u_{method} includes all uncertainty components originating from each working step along the workflow, including air sampling and quantitative analysis of the collected aerosol, and is calculated according to formula (4):

$$u_{method} = \sqrt{u_{sampling}^2 + u_{analytical}^2} \quad (4)$$

The combined method standard uncertainty is multiplied by a coverage factor k to obtain the method expanded uncertainty. Here, k is chosen to be 2. The resulting expanded method uncertainty provides an interval that is expected to encompass the distribution of measurement values that can be attributed to the measurand with a confidence of approximately 95%.

Figure S13 shows the calculated uncertainty components as a function of mass for (A) SWCNT and (B) MWCNT (Table S10 and Table S11). The expanded method uncertainty for SWCNT takes the form of a U and is ~30% at the extremes of the instrument working range, and ~25% in the intermediate range. The MWCNT data shows a decreasing expanded method uncertainty with increasing nominal mass from ~41% at 0.5 ng to a constant 25% at masses exceeding 10 ng MWCNT. The top x-axes in Figure S13 indicate the REL fractions (NIOSH REL for CNT at 1 µg/m^3) calculated for corresponding 8-hour samplings at 20% intermittence (i.e. 20% of total sampling time with 40s-pump-on, 160s-pump-

off cycles) and the nominal flow rate of the sampler. The data for both types of CNT shows compliance with the requirements defined in ISO 20581:2016.

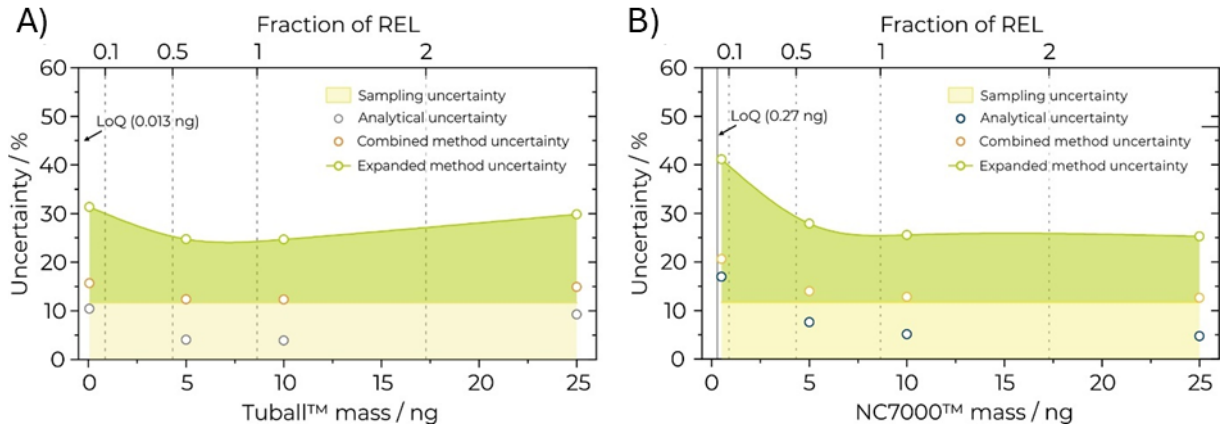

Figure S13. Uncertainty components contributing to method uncertainty for Tuball™ SWCNT (a) and NC7000™ MWCNT (b). The expanded method uncertainty is calculated using a coverage factor of 2 (k = 2). The calculated fraction of REL (top x-axes) is calculated for an 8-hour sampling at 20% intermittence and a REL = 1 µg/m^3. The green lines are the results of spline interpolations.

Figure S13 further shows the corresponding LoQ values for SWCNT and MWCNT. In both cases, a measurement at the LoQ has an associated expanded method uncertainty below 50%. The upper method working range, in turn, is limited by extinction effects, leading to deviations from the linear Raman signal response above 25 ng. Consequently, the method working ranges for SWCNT and MWCNT coincide with the respective instrument working ranges as determined above, as the expanded method uncertainty does not impose any further restrictions.

The method working range for Tuball™ SWCNT is from 0.013 - 25 ng, thereby covering more than three orders of magnitude. The corresponding concentration range accessible with this method is 0.0015 - 2.89 µg/m^3 or 0.0015 - 2.89 times the REL in 8-hour samplings at 20% intermittence. The corresponding range for NC7000™ MWCNT is from 0.27 - 25 ng, thereby covering almost two orders of magnitude. The accessible concentration range is 0.03 - 2.89 µg/m^3 or 0.03 - 2.89 times the REL in 8-hour samplings at 20% intermittence.

Table S10. Summary of uncertainty components for SWCNT contributing to the method uncertainty, and expanded method uncertainty using a coverage factor of $k = 2$.

Nominal mass (ng)	Sampling uncertainty (%)	Analytical uncertainty (%)	Combined method standard uncertainty (%)	Expanded method uncertainty (%)
0.05	11.7	10.4	15.7	31.3
5	11.7	4.0	12.4	24.7
10	11.7	3.9	12.3	24.7
25	11.7	9.2	14.9	29.8

Table S11. Summary of uncertainty components for MWCNT contributing to the method uncertainty, and expanded method uncertainty using a coverage factor of $k = 2$.

Nominal mass (ng)	Sampling uncertainty (%)	Analytical uncertainty (%)	Combined method standard uncertainty (%)	Expanded method uncertainty (%)
0.5	11.7	16.9	20.6	41.1
5	11.7	7.6	13.9	27.9
10	11.7	5.1	12.8	25.6
25	11.7	4.7	12.6	25.3

S6 – Derived recommendations for risk minimisation

In view of the increasing volumes of battery waste and associated OHS concerns, the aerosol measurements conducted in this study indicate that mechanical battery recycling processes can lead to an exposure to fine and ultrafine particles. SMPS measurements showed that comminution processes of electrode material on a laboratory scale resulted in nanoparticle exposure levels below 1'000 nanoparticles per cm^3, which is markedly lower than particle number concentrations reported for nanomaterial and CNT manufacturing facilities (Falta et al., 2022). By comparison, industrial processes such as hard metal powder production or CNT manufacturing can yield in particle number concentrations of up to 10'000 or 41'000 nanoparticles per cm^3, respectively (Falta et al., 2022).

The results of the MWCNT release at the laboratory scale, which are based on a previously described quantification method, showed that the TWA concentrations were above the NIOSH recommended exposure limit (REL) of 1 $\mu g/m^3$ of respirable CNTs. In contrast, the SWCNT results were below the REL. During the simulated recycling activities, the test MWCNT battery cells and the SWCNTs cells showed only minor differences in the release of UFPs and nanofibers. Notably, the exposure to fine particles (PM_{10}) during the shredding process of MWCNT cells was higher than during shredding of SWCNT cells. However, further research is needed to gain a better understanding of the release mechanism and potential risks to human health, and more case studies are needed, particularly in large-scale industrial settings. Although the results from the laboratory experiments cannot be transferred to industrial scales, we recommend the following general measures for larger industrial plants:

- Installation of encapsulated systems for the mechanical processing of (lithium-ion) batteries with multiple filter stages to avoid any emissions of fine and ultrafine particles and respirable nanofibers.
- Compliance with organisational protective measures, such as limiting the number of exposed employees and limiting the duration and/or intensity of exposure, restricting access to exposed areas, and implementing sufficient general occupational hygiene measures.
- Training of workers in production and recycling facilities to raise awareness of the potential risks associated with nanomaterials and other potential hazardous substances throughout the product life cycle of batteries, which may feature different cell chemistries and material compositions.
- Use of personal protective equipment (PPE) to minimise the risks associated with inhaling nanomaterials and dermal contact. This includes the use of FFP3 masks, gloves, safety glasses and protective coats.

References

Birch, E., Wang, C., Fernback, J. E., Feng, H. A., Birch, Q. T., & Dozier, A. K. (2017). Analysis of Carbon Nanotubes and Nanofibers on Mixed Cellulose Ester Filters by Transmission Electron Microscopy. NIOSH Manual of Analytical Methods (NMAM), 5th Edition.

CEN. (2014). EN 13205-2:2014 - Workplace exposure - Assessment of sampler performance for measurement of airborne particle concentrations - Part 2: Laboratory performance test based on determination of sampling efficiency. European Committee for Standardization (CEN).

Currie, L. A. (1999). Nomenclature in evaluation of analytical methods including detection and quantification capabilities1Adapted from the International Union of Pure and Applied Chemistry (IUPAC) document "Nomenclature in Evaluation of Analytical Methods including Detection and Quantification Capabilities", which originally appeared in Pure and Applied Chemistry, 67 1699–1723 (1995) © 1995 IUPAC. Republication permission granted by IUPAC.1: (IUPAC Recommendations 1995). *Analytica Chimica Acta*, *391*(2), 105–126. https://doi.org/https://doi.org/10.1016/S0003-2670(99)00104-X

Dresselhaus, M. S., Dresselhaus, G., Saito, R., & Jorio, A. (2005). Raman spectroscopy of carbon nanotubes. *Physics Reports*, *409*(2), 47–99. https://doi.org/https://doi.org/10.1016/j.physrep.2004.10.006

Dresselhaus, M. S., Jorio, A., Hofmann, M., Dresselhaus, G., & Saito, R. (2010). Perspectives on Carbon Nanotubes and Graphene Raman Spectroscopy. *Nano Letters*, *10*(3), 751–758. https://doi.org/10.1021/nl904286r

Falta, T., Fries, R., Gazso, A., Graff, A., Lehr, S., Orsolits, G., Part, F., Pavlicek, A., & Rose, G. (2022). M.plus 310 Nanomaterialien. Allgemeine Unfallversicherungsanstalt (AUVA). Vienna, Austria. URL: https://auva.at/praevention/medien-und-publikationen/publikationen-us/mplus-310-nanomaterialien/ (last access on 14.11.2024).

Hasegawa, K., & Noda, S. (2016). Lithium ion batteries made of electrodes with 99 wt% active materials and 1 wt% carbon nanotubes without binder or metal foils. *Journal of Power Sources*, *321*, 155–162. https://doi.org/https://doi.org/10.1016/j.jpowsour.2016.04.130

ISO. (1995). ISO 7708:1995. Air quality - Particle size fraction definitions for health-related sampling. International Organization for Standardization (ISO).

ISO. (2016). ISO 20581:2016. Workplace air — General requirements for the performance of procedures for the measurement of chemical agents. International Organization for Standardization (ISO).

Landi, B. J., Ganter, M. J., Cress, C. D., DiLeo, R. A., & Raffaelle, R. P. (2009). Carbon nanotubes for lithium ion batteries [10.1039/B904116H]. *Energy & Environmental Science*, *2*(6), 638–654. https://doi.org/10.1039/B904116H

Li, X., Kang, F., & Shen, W. (2006). A Comparative Investigation on Multiwalled Carbon Nanotubes and Carbon Black as Conducting Additive in LiNi0.7Co0.3O2. *Electrochemical and Solid-State Letters*, *9*(3), A126. https://doi.org/10.1149/1.2161442

Liang, Y., Zhao, C.-Z., Yuan, H., Chen, Y., Zhang, W., Huang, J.-Q., Yu, D., Liu, Y., Titirici, M.-M., Chueh, Y.-L., Yu, H., & Zhang, Q. (2019). A review of rechargeable batteries for portable electronic devices. *InfoMat*, *1*(1), 6–32. https://doi.org/https://doi.org/10.1002/inf2.12000

López-Lorente, A. I., Simonet, B. M., Valcárcel, M., & Mizaikoff, B. (2013). Bare gold nanoparticles mediated surface-enhanced Raman spectroscopic determination and quantification of carboxylated single-walled carbon nanotubes. *Analytica Chimica Acta*, *788*, 122–128. https://doi.org/https://doi.org/10.1016/j.aca.2013.06.008

Meyer-Plath, A., Bäger, D., Dziurowitz, N., Perseke, D., Simonow, B. K., Thim, C., Wenzlaff, D., & Plitzko, S. (2020). A Practicable Measurement Strategy for Compliance Checking Number Concentrations of Airborne Nano- and Microscale Fibers. *Atmosphere*, *11*(11). https://doi.org/10.3390/atmos11111254

Petersen, E. J., Flores-Cervantes, D. X., Bucheli, T. D., Elliott, L. C., Fagan, J. A., Gogos, A., Hanna, S., Kagi, R., Mansfield, E., Bustos, A. R., Plata, D. L., Reipa, V., Westerhoff, P., & Winchester, M. R. (2016). Quantification of Carbon Nanotubes in Environmental Matrices: Current Capabilities, Case Studies, and Future Prospects. *Environ Sci Technol*, *50*(9), 4587–4605. https://doi.org/10.1021/acs.est.5b05647

Saito, R., Hofmann, M., Dresselhaus, G., Jorio, A., & Dresselhaus, M. S. (2011). Raman spectroscopy of graphene and carbon nanotubes. *Advances in Physics*, *60*(3), 413–550. https://doi.org/10.1080/00018732.2011.582251

Salzmann, C. G., Chu, B. T. T., Tobias, G., Llewellyn, S. A., & Green, M. L. H. (2007). Quantitative assessment of carbon nanotube dispersions by Raman spectroscopy. *Carbon*, *45*(5), 907–912. https://doi.org/https://doi.org/10.1016/j.carbon.2007.01.009

Tsai, C. S.-J., & Theisen, D. (2018). A sampler designed for nanoparticles and respirable particles with direct analysis feature. *Journal of Nanoparticle Research*, *20*(8), 209. https://doi.org/10.1007/s11051-018-4307-2

Wang, G., Li, H., Zhang, Q., Yu, Z., & Qu, M. (2011). The study of carbon nanotubes as conductive additives of cathode in lithium ion batteries. *Journal of Solid State Electrochemistry*, *15*(4), 759–764. https://doi.org/10.1007/s10008-010-1143-4

Williams, A., & Ellison, S. L. R. (2012). EURACHEM / CITAC Guide CG 4. Quantifying Uncertainty in Analytical Measurement. Third Edition. https://www.eurachem.org/images/stories/Guides/pdf/QUAM2012_P1.pdf (last access on 7.1.2026).

Yoo, J.-K., Oh, Y., Park, T., Lee, K. E., Um, M.-K., & Yi, J.-W. (2019). Optimization of Carbon Nanotubes as Conductive Additives for High-Energy-Density Electrodes for Lithium-Ion Batteries. *Energy Technology*, *7*(5), 1800845. https://doi.org/https://doi.org/10.1002/ente.201800845

Zumwalde, R., Kuempel, E., Birch, E., Trout, D., & Castranova, V. (2013). Occupational exposure to carbon nanotubes and nanofibers. *Current Intelligence Bulletin*, *65*(2013-145).